TECHNISCHE MECHANIK
an open access journal

journal homepage: www.ovgu.de/techmech

Tech. Mech., Vol. 44, Is. 2, (2024), 110–121

Received: 10.07.2024
Accepted: 29.07.2024
Available online: 29.07.2024

Numerical and experimental considerations of non-linearities for a trifilar pendulum

M. Meywerk[1]* and T. Hellberg[1]

[1] Helmut Schmidt University, University of the Federal Aremd Forced, Institute for Automotive and Powertrain Engineering, Holstenhofweg 85, Postfach 700822, 22043 Hamburg, Germany

Abstract: Moments of inertia of machine-components or whole machines are essential for numerical simulations, especially for Mutli-Body-Simulations. Various measuring techniques exists, which can be rougly divided in techniques using oscillations or accelerations. One possibility to measure indirectly the inertia properties are multifilar pendulums, for example the trifilar pendulum using a platform and three ropes or filars. A lot of literature dealing with the trifilar pendulums exists. We will give a brief overview of the literature with emphasis to non-linearities. Furthermore, we will investigate nonlinear effects and compare them with experimental and numerical results.

Keywords: Moment of inertia measuring, trifilar pendulum, non-linearities, experiment, numerical investigation.

1 Introduction

In the first subsection we will give an overview of possible measurement techniques for inertia properties, in the second subsection we will give a brief literature overview concerning multifilar pendulums.

1.1 Experimental Investigations of Moments of Inertia

An overview of experimental techniques for measuring the moments of inertia is shown in Fig. 1. The techniques can be subdivided in experiments using accelerations and experiments using oscillations of the object of investigation. The acceleration experiments are not appropriate or difficult to apply for a broad range of specimens. As well, not all oscillatory experimental techniques are easy to apply (for more details s. Genta and Delprete (1994)). Three of the oscillatory investigation methods are frequently used in industry or research: linear or torsion spring test rigs, servohydraulic devices and multifilar pendulums. Some characteristics of these three techniques are shown in Table 1, they are exemplary described in Wegener (2012) (oscillation: active), in Klöpper et al. (2013) (oscillation: passive) or in Gobbi et al. (2011) (multifilar pendulum). To distinguish the three methods, we call the first two ”oscillation”, passive and active, and the third one multifilar pendulum; of course, the multifilar pendulum is as well a passive oscillation method.

The multifilar pendulum is one of the cost-efficient ways, but for industrial practice it is not very convenient. It may take a long measurement time and there might be some pitfalls, e.g. neglecting the kinetic translational kinetic energy or bending and/or torsion stiffness of the filars, choosing unfavourable geometry (short length of the filars), positioning the centre of mass of the object of investigation not on the centre line of the pendulum, having large translational oscillations of the pendulum. Therefore, the easy-to-use but expensive techniques enter in the industrial daily routine. One important difference between the first two techniques (here called oscillation) and the third one is, that method 1 and 2 need to be calibrated, whereas for method 3 the moment of inertia can be calculated from time, length, mass measurements, and the geometry of the platform with physical principles.

In the remaining part of this article we focus on the trifilar pendulum, and we focus on the calculation of the time period and its governing equation.

Tab. 1: Qualitative comparison of some experimental techniques

	1. Oscillation (passive)	2. Oscillation (active)	3. Multifilar Pendulum
Price	moderate	very high	low
Usability	Sufficiently easy	Sufficiently easy	Not easy
Friction/damping	Not documented	Not documented	can be considered
10 inertia prop.	Yes (one measurement)	Yes (one measurement)	Yes, more measurements
(Non)-linear?	linear	linear	Non-linear possible

* E-mail address: martin.meywerk@hsu-hh.de
doi: 10.24352/UB.OVGU-2024-059

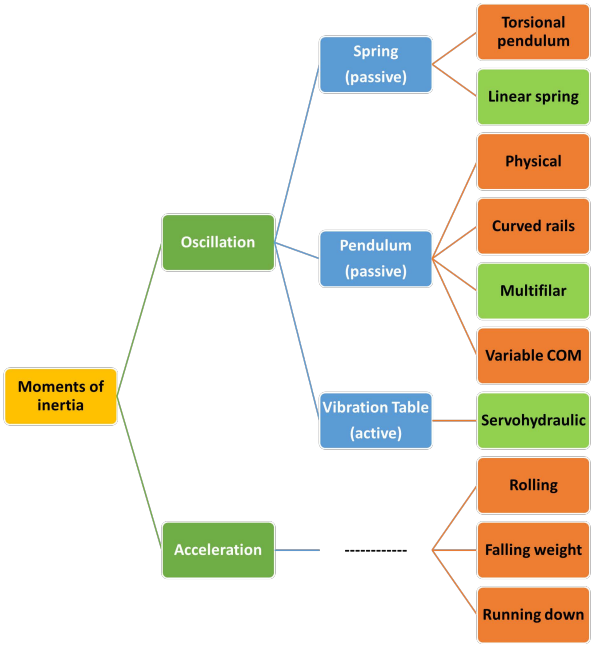

Fig. 1: Overview of measuring techniques of the moments of inertia (cf. Genta and Delprete (1994)).

1.2 Literature

Publications dealing with multifilar pendulums (mainly bifilar pendulums) for determining physical quantities, e.g. the magnetic field of the earth (cf. Gauß (1838), Kohlrausch (1882)), the moments of inertia of a body or the acceleration of gravity (cf. Klopsteg (1930)) are published early in the scientific community. There are a lot of publications, and we will not give a complete overview, but we want to give some hints to famous, important and as well two doubtful publications; those readers, who want to apply multifilar pendulums for measurement aims should be aware of the latter type of publications.

A famous application of multifilar pendulums is the bifilar magnetometer which was described in Gauß (1838). In his description, the non-linearity of the period T with respect to the amplitude is given on p. 66, where G is twice the amplitude of the angle:

$$T = T' \left(1 + \frac{1}{4}\sin^2\left(\frac{1}{4}G\right) + \frac{1}{4}\cdot\frac{9}{16}\sin^4\left(\frac{1}{4}G\right) + \frac{1}{4}\cdot\frac{9}{16}\cdot\frac{25}{36}\sin^6\left(\frac{1}{4}G\right) + \ldots\right) \tag{1}$$

Peculiar, Gauß cited the equation, which holds for the mathematical pendulum (Dreizler and Lüdde (2008), p. 167) and this equation results from a series expansion for the elliptic integral [1] ($G = 2\varphi_0$, where φ_0 is the amplitude of the pendulum oscillation, T is the period for large amplitudes φ_0, and T' is the period for infinitesimal small amplitudes, $T' = \lim_{\varphi_0 \to 0} T$).

The qualitative behaviour of the period-amplitude-dependency $T = T(\varphi_0)$ (thus, the time T increases with an increasing amplitude φ_0) is correct in Gauß (1838). But the correct physical quantities, i.e. the distance $2R$ between (the parallel) filars, the length L of the filars and the radius of gyration $r_g = \sqrt{J/M}$ (J and M are the moment of inertia or the mass, resp., of the rotating part at the end of the filars) enter not in this equation. Some of the older publications, e.g. Auerbach (1908), states the reverse qualitative dependency between T and φ_0, i.e. a decreasing period T with increasing amplitude φ_0, which is not correct.

In Uhler (1923) the governing equation for a bifilar pendulum is given, and a series expansion for the undamped pendulum using conservation of energy (i.e. the Hamiltonian) is developed.

Genta and Delprete (1994) gives an overview of measurement techniques with an emphasis to error analysis. They concluded, that among the oscillatory methods the torsional and the multifilar pendulum are more accurate and an error smaller than 1% is accessible. In the appendix they give a non-linear equation of motion. In the derivation of this equation, the kinetic energy from the vertical motion is not considered.

Hou et al. (2009) describes a method to identify ten parameters (six of the tensor of moments of inertia, the mass, and the coordinates of the centre of mass) by placing the object of investigation in nine different positions and orientations on the oscillation platform of a trifilar pendulum. The aspect of elongation of the filars are taken into account. They use the simplified, linear equation for the calculation of the moments of inertia.

In Lyons (2002) the linear theory is favoured for the identification of the moments or inertia. The parasitic, translational oscillation perpendicular to the axis of rotation is mentioned as one possible reason for inaccurate measurement of the period of time; the solution, they suggest, is averaging over a large number of oscillation cycles. They give a calculation method using the Hamiltonian for the non-linear equation, but they do not take into account the translational kinetic energy for the motion in the vertical direction.

[1] Here, the period $T = \frac{4}{\omega}\int_0^{x/2} \frac{\mathrm{d}s'}{\sqrt{1-k^2\sin^2 s'}}$ is calculated using the series expansion $\frac{1}{\sqrt{1-k^2\sin^2 s'}} = 1 + \frac{1}{2}k^2\sin^2 s' + \frac{3}{8}k^4\sin^4 s' + \frac{5}{16}k^6\sin^6 s' + \ldots$ and $\int_0^{\pi/2}\sin^{2n} s'\mathrm{d}s' = \frac{1\cdot3\cdot5\cdots(2n-1)}{2\cdot4\cdot6\cdots2n}\frac{\pi}{2}$, $\omega = \sqrt{g/\ell}$ is the angular frequency of the linearised equation for the pendulum and $k = \sin(\varphi_0/2)$ with φ_0 the amplitude of the oscillation angle of the pendulum (Dreizler and Lüdde (2008), p. 167).

1.3 Goal

The goal of this paper is the experimental determination of moments of inertia of rigid bodies. For this purpose, the body is placed on a platform, which is symmetrically supported by three filars (we use wire ropes). We show the inertia calculation of this trifilar pendulum based on the period duration of the rotational oscillation. For this procedure, a method for compensating bending stiffness and elongation is explained and numerically evaluated for the linear and the non-linear approach. A numerical investigation of the complete equation for the period is given. Some approaches from literature are compared.

2 Experiment

The experimental setup is shown in Fig. 2. A support frame mounted at the top of the laboratory is the carrier of the trifilar pendulum. There are three load cells mounted to the frame. Each filar (steel wire rope) is clamped at one load cell. The lengths of the filars are $L \approx 11$ m; the actual length during a measurement depends on the mass of the object of investigation, and, therefore, the lengths are measured using a laser distance sensor. The aim of the load cells is, that the centre of mass of the object of investigation is well-positioned on the centre line (z-axis) of the platform, i.e., all load cells measure the same force in the resting position. The wire ropes are mounted to the platform by spherical-like joints. This means, that except of friction, neither bending nor torsion torques are acting on the lower end of the filars. The platform carries the object of investigation.
The moments of inertia J with respect to the z-axis are indirectly measured by measuring the period time of rotational oscillation (short: period T_{exp}) with respect to the z-axis. This period then is used to calculate J.
In a preliminary step the period T_{pre} of the unloaded platform is measured; in this measurement, all parts including the wire ropes, enter into the measurement. From T_{pre} the moment of inertia J_{un} of the unloaded platform is calculated (s. Sect. 3).
Once J_{un} is calculated, the period T_{exp} of the loaded platform is measured, and with T_{exp} the moment of inertia J_{lo} of the loaded platform is calculated. As the moment of inertia is additive, the moment of inertia of the object of investigation is:

$$J = J_{lo} - J_{un} \quad . \tag{2}$$

For the calculation of the moment of inertia, the lengths of the filars and the masses of the unloaded platform and of the object of investigation must be measured, as well.

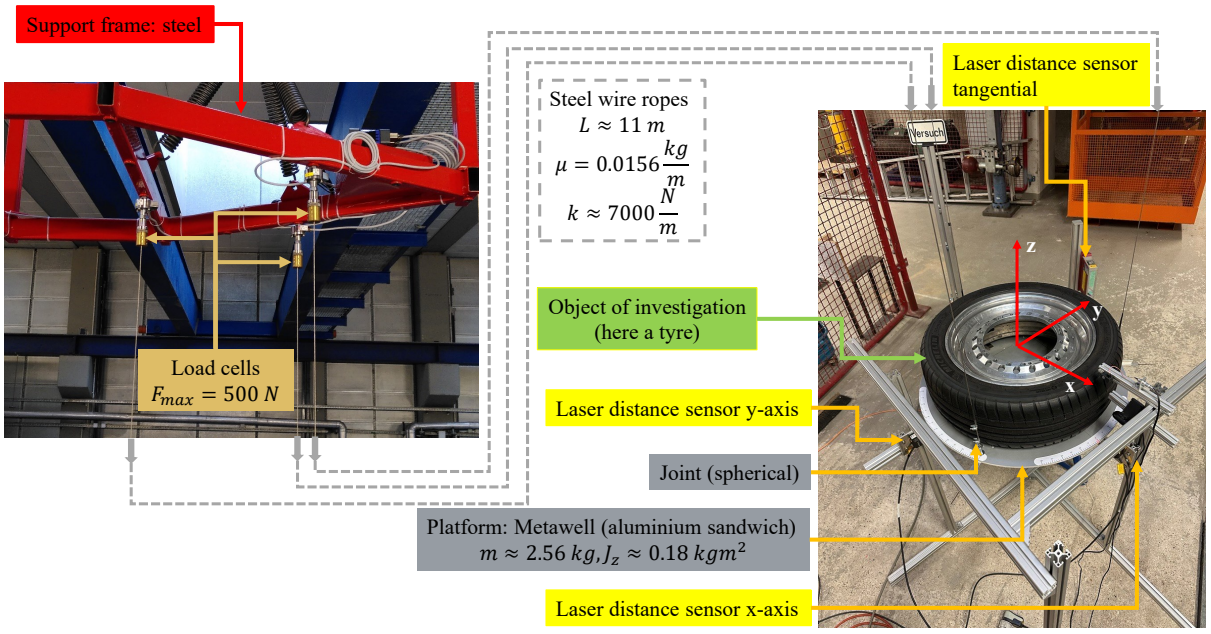

Fig. 2: Experimental setup of the trifilar pendulum.

3 Theory

In this section we will establish the governing equations for the ideal trifilar pendulum, and we will discuss some perturbations of the ideal case; more perturbations or uncertainties are described in the literature, e.g. in Genta and Delprete (1994).

3.1 Equation of Motion and Period

In Fig. 3 a schematic sketch of the idealized trifilar pendulum is shown. It consists of the platform (which supports the object of investigation) and the three filars. In grey the system is shown in the not deflected position of rest. In the deflected position the

filars are red and the platform is yellow. For the derivation of the equations of motion and for the calculation of the period we use energetic approaches. We describe merely the rotational degree of freedom with respect to the $\vec{e}_z$-axis by the angle φ[2].

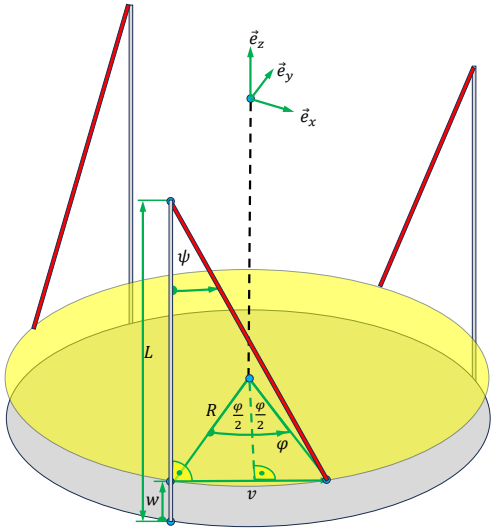

Fig. 3: Idealized model of the trifilar pendulum.

We obtain the dependency of w with respect to φ from the three right-angled triangles in Fig. 3 and some trigonometric transformation

$$w(\varphi) = L\left(1 - \sqrt{1 - 4\xi^2 \sin^2\frac{\varphi}{2}}\right) \tag{3}$$

$$= L\left(1 - \sqrt{1 - 2\xi^2(1 - \cos\varphi)}\right) \tag{4}$$

where

$$\xi = \frac{R}{L} \ . \tag{5}$$

For the energies, we have to take into account the rotational and translational kinetic parts, T_r and T_t resp., as well as the potential energy U:

$$T_r = \frac{1}{2}J\dot{\varphi}^2 \ , \tag{6}$$

$$T_t = \frac{1}{2}M\dot{w}^2 \ , \tag{7}$$

$$U = Mg(w - w_0) \ . \tag{8}$$

Here J is the moment of inertia of the rotating part, i.e. the platform, the object of investigation and the filars, M is the corresponding mass and g is the gravitational acceleration.
The value w_0 corresponds to the amplitude φ_0 of the rotational oscillation, which means, that the system has no kinetic energy in the position $w = w_0$ and $\varphi = \varphi_0$. From the principle of conservation of energy, we obtain, that the Hamiltonian $\mathcal{H}$ is zero ($T_{tot} = T_r + T_t$):

$$\begin{aligned}\mathcal{H} &= T_{tot} + U \\ &= \frac{1}{2}J\dot{\varphi}^2 + \frac{1}{2}M\dot{w}^2 + Mg(w - w_0) \\ &= \frac{1}{2}J\dot{\varphi}^2 + \frac{1}{2}M\left(\frac{\partial w}{\partial\varphi}\dot{\varphi}\right)^2 + Mg(w - w_0) \\ &= \frac{1}{2}f(\varphi)\dot{\varphi}^2 + Mg(w - w_0) = 0 \ ,\end{aligned} \tag{9}$$

where

$$f(\varphi) = J + M\left(\frac{\partial w}{\partial\varphi}\right)^2 \tag{10}$$

$$= J + M\frac{R^4 \sin^2\varphi}{L^2\left(1 - 2\xi^2(1 - \cos\varphi)\right)} \tag{11}$$

[2] Uhler (1923) stated, that the angle ψ between the filars and the vertical resting position of the filars yield simpler equations, which is correct; we prefer the more descriptive angle φ. An alternative variable is the elevation w.

Rearranging (9) yields:

$$\dot{\varphi} = \pm\sqrt{\frac{2Mg(w - w_0))}{f(\varphi)}} \tag{12}$$

Restricting the consideration to a quarter of the oscillation period T we obtain from Eq. (9) by separation of the variables (cf. Awrejcewicz (2012), p. 71, or Uhler (1923)):

$$\int_0^{\varphi_0} \sqrt{\frac{f(\varphi)}{2Mg(w - w_0))}}\,\mathrm{d}\varphi = \int_0^{T/4} \mathrm{d}t = \frac{T}{4} \tag{13}$$

where φ_0 is the amplitude of the oscillation.
The period time T with respect to the amplitude φ_0 for the undamped pendulum then is:

$$T(\varphi_0) = 4\int_0^{\varphi_0} \sqrt{\frac{\frac{J}{M}L^2\left(1 - 2\xi^2(1 - \cos\varphi)\right) + R^4\sin^2\varphi}{2gL^3\left(1 - 2\xi^2(1 - \cos\varphi)\right)\left(\sqrt{1 - 2\xi^2(1 - \cos\varphi)} - \sqrt{1 - 2\xi^2(1 - \cos\varphi_0)}\right)}}\,\mathrm{d}\varphi \tag{14}$$

The integral looks similar to hyperelliptic integrals, which we solve numerically only. For the numeric integration it is important, that the denominator has a zero at $\varphi = \varphi_o$.
For the determination of the moment of inertia J, the zero of $T - T_{exp}$ is determined: As T is strictly monotonic increasing with increasing J, the determination of the zero is straightforward.
Additional to Eq. (14) for the period, we derive the equation of motion by applying the formalism of Lagrange. The Lagrangian is:

$$\mathcal{L} = \frac{1}{2}f(\varphi)\dot{\varphi}^2 - Mg(w - w_0) \tag{15}$$

Applying the Euler-Lagrange equation to Eq. (15)

$$\frac{\mathrm{d}}{\mathrm{d}t}\frac{\partial\mathcal{L}}{\partial\dot{\varphi}} - \frac{\partial\mathcal{L}}{\partial\varphi} = 0 \tag{16}$$

yields the equation of motion:

$$\ddot{\varphi}f(\varphi) + \frac{1}{2}\dot{\varphi}^2\frac{\partial f}{\partial\varphi} + Mg\frac{\partial w}{\partial\varphi} = 0\ . \tag{17}$$

With

$$\frac{\partial w}{\partial\varphi} = L\frac{\xi^2\sin\varphi}{\sqrt{1 - 2\xi^2(1 - \cos\varphi)}} \tag{18}$$

and (11) we obtain the linearised form of the equation of motion:

$$J\ddot{\varphi} + \frac{MgR^2}{L}\varphi = 0 \tag{19}$$

which results in the period time T' of the linearised system:

$$T' = \frac{2\pi}{R}\sqrt{\frac{JL}{Mg}}\ . \tag{20}$$

3.2 Torque from filar bending and torsion

Although the filars of a multifilar pendulum are usually very thin, they have an influence on the period T, which might be not negligible. In this subsection we have a closer look to the additional restoring torque resulting from bending of the filars. The filars could be wire ropes or single wires. The latter one can be treated like a simple slender beam or bar, the mechanical behaviour of the wire rope is more complicated, but bending is significantly smaller than for comparable slender beams.
The type of the joints between the filars and the platform on the bottom side and the frame on the top side is essential for the restoring torque:

1. If spherical joints are on both ends of the filars, there are no moments, neither from bending nor from torsion, at the ends of the filars, which results in no restoring torque.

2. If one end is clamped and the other end is jointed by a spherical joint, then this filar is equivalent to a clamped beam (without torsion), where the deflection v is (cf. Fig. 3):

$$v(\varphi) = 2R \sin \frac{\varphi}{2} \tag{21}$$

In the case of a single wire (slender beam: bending stiffness EI; E Young's modulus, $I = \pi r^4/4$ second moment of the circular cross section with radius r of the filar), the deflection v of one filar results in a restoring force F_{rest} of (here we use the maximum deflection of a one-sided clamped Euler Bernoulli beam with bending stiffness EI of length L loaded by a force F at the free end, which is $FL^3/(3EI)$)

$$F_{\text{rest}} = \frac{3EI2R \sin \frac{\varphi}{2}}{L^3} \tag{22}$$

which yields for N filars ($N = 2$ for a bifilar and $N = 3$ for a trifilar pendulum) a restoring torque M_{rest}:

$$M_{\text{rest}} = N \frac{3EI2R^2 \sin \frac{\varphi}{2}}{L^3} \tag{23}$$

or linearised for small angles φ:

$$M_{\text{rest}} \approx N \frac{3EIR^2\varphi}{L^3} \tag{24}$$

3. If both sides are clamped, the deformation is S-shaped and due to symmetry we obtain one portion of the restoring torque from bending

$$F_{\text{rest}} = \frac{3EIR \sin \frac{\varphi}{2}}{(L/2)^3} \tag{25}$$

$$M_{\text{rest,b}} = N \frac{3EIR^2 \sin \frac{\varphi}{2}}{(L/2)^3} \tag{26}$$

$$M_{\text{rest,b}} \approx N \frac{3EIR^2\varphi}{2(L/2)^3} \tag{27}$$

Furthermore, an additional portion results from torsion

$$M_{\text{rest,t}} = N \frac{GI_p\varphi}{L} \tag{28}$$

The relation between the two torques are ($G = E/2(1+\nu)$, $I_p = 2I$):

$$\frac{M_{rest,t}}{M_{\text{rest,b}}} = \frac{L^2}{12R^2(1+\nu)} \tag{29}$$

For $L > \sqrt{12(1+\nu)}R$ the restoring torque from torsion is larger than the torque from bending. In our setup, if we would have such a kind of joint of the filars, we have ($L \approx 11m$ and $R = 0.33m$): $L^2/(12R^2(1+\nu)) \approx 71$.

4. If one end is clamped and on the other end is a revolute joint as rotator (swivel), there is no torque from torsion but only from bending like in case 3.

We discuss the second case (which we have in our experimental setup; $N = 3$) in more detail for the linearised equation of motion. Due to the additional restoring torque, the equation of motion is:

$$J\ddot{\varphi} + \xi^2 \left(LMg + N\frac{3EI}{L} \right) \varphi = 0 \tag{30}$$

The periodic time of the linearised and extended equation is:

$$T' = \frac{2\pi}{R} \sqrt{\frac{JL}{Mg}} \frac{1}{\sqrt{1 + N\frac{3EI}{L^2Mg}}} \tag{31}$$

The length L of the pendulum depends on the weight Mg and on the axial stiffness EA ($A = \pi r^2$ area of the cross section) of the filars. This results in an elongation ΔL of the pendulum ($L = L_0 + \Delta L$):

$$\Delta L = L_0 \frac{Mg}{NEA} \tag{32}$$

Thus, we have two effects: one from the bending stiffness, which decreases the time period, and one of the axial stiffness, which increases the time period. A series expansion of the square root in (31) results in:

$$T' = \frac{2\pi}{R}\sqrt{\frac{J(L_0+\Delta L)}{Mg}}\left(1+N\frac{3EI}{L^2Mg}\right)^{-\frac{1}{2}} \tag{33}$$

$$= \frac{2\pi}{R}\sqrt{\frac{JL_0}{Mg}}\left(1+\frac{Mg}{NEA}\right)^{\frac{1}{2}}\left(1+N\frac{3EI}{L^2Mg}\right)^{-\frac{1}{2}} \tag{34}$$

$$= \frac{2\pi}{R}\sqrt{\frac{JL_0}{Mg}}\left(1+\frac{1}{2}\frac{Mg}{NEA}-\frac{1}{8}\left(\frac{Mg}{NEA}\right)^2+\ldots\right)\left(1-\frac{1}{2}N\frac{3EI}{L^2Mg}+\frac{3}{8}\left(N\frac{3EI}{L^2Mg}\right)^2+\ldots\right) \tag{35}$$

$$= \frac{2\pi}{R}\sqrt{\frac{JL_0}{Mg}}\left(1+\underbrace{\frac{1}{2}\frac{Mg}{NEA}-\frac{1}{2}N\frac{3EI}{L^2Mg}}_{=e_1}+\ldots\right) \tag{36}$$

The first order term e_1 is ($I=\pi r^4/4$, $A=\pi r^2$, setting $L=L_0+\Delta L$ and series expansion yield higher order terms with ΔL):

$$e_1 = \frac{Mg}{2NE\pi r^2}\left(1-\frac{3\left(NE\pi r^3\right)^2}{\left(2L_0Mg\right)^2}\right) \tag{37}$$

(38)

For fixed length L and Young's modulus E of the filars, the two nonlinear effects compensate each other in the first order for a specific radius r of the filars, which depends on the mass M (platform and object of investigation); this radius r_{opt} is given by:

$$r_{opt} = \sqrt[3]{\frac{2LMg}{\sqrt{3}NE\pi}} \tag{39}$$

The error e_1 is (numerically nearly) zero, if the radius r is chosen individually following Eq. (39) for each mass (cf. Fig. 4 a). This is inconvenient or impossible for everyday laboratory work. Therefore, we choose a radius from Eq. (39) for a mass in the centre of our interval, i.e. $M \approx 22.9$ kg, and obtain the first order error for this fixed radius (for each of the length L), which is shown in Fig. 4 b). The first order error remain small, especially for $L = 10$ m. Thus, this compensation works very well for a long pendulum. But if we look to the normal stresses in the filars, Fig. 4 c), we see quite large stresses, for $L = 10$ m up to 119 MPa and for $L = 1$ m up to 556 MPa. Choosing appropriate steel, both values do not exceed the elastic stress limit. But during the placement of the object of investigation on the platform, especially for large masses, the risk of a shock on the platform can result in plastic deformation of one or more filars, which results in different lengths of the filars and the necessity to replace them. A crack of one filar results in hazard situation, where the object of investigation drops down and may injure the experimenter.
Therefore, we did not implement the compensation of bending and elongation in our experimental setup and the analysis of the experiments. Instead of this, we use wire ropes with very small bending stiffness and large elastic stresses and tensile strength. Because the wire ropes show large elongation, we measure the length of the filars for each object of investigation individually by a laser measurement device.

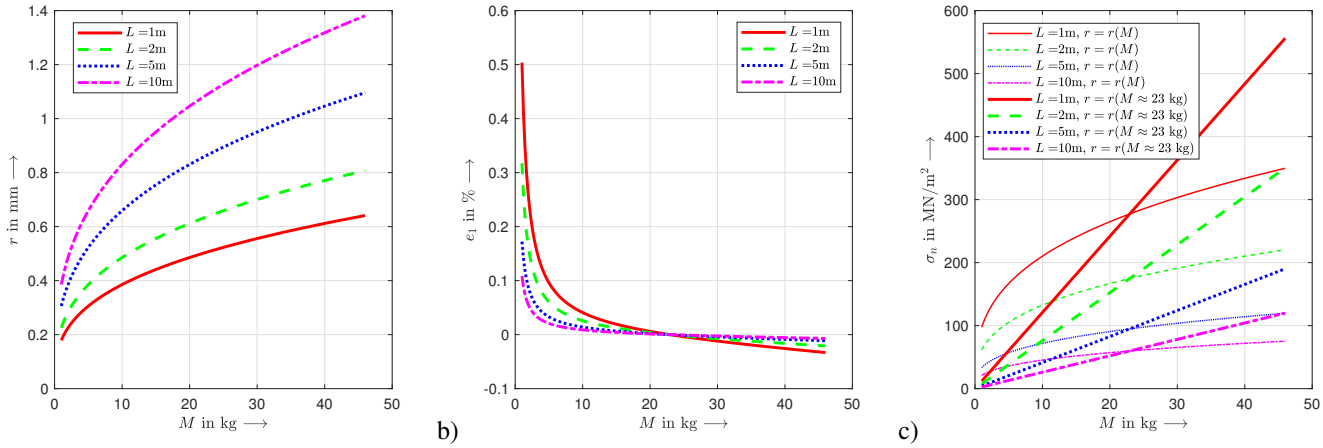

Fig. 4: Idealized model of the trifilar pendulum.

The equation for the time period Eq. (14) can be extended; from Eq. 21, $v(\varphi) = 2R\sin\frac{\varphi}{2}$, we obtain

$$\frac{\mathrm{d}v}{\mathrm{d}\varphi} = R\cos\frac{\varphi}{2} \tag{40}$$

which yield the potential energy U_{fil} of he filars by integration of Eq. (22)

$$U_{fil}(\varphi) = N\frac{6EIR^2}{L^3}\int_0^{\varphi} \sin\frac{\varphi'}{2}\cos\frac{\varphi'}{2}\,\mathrm{d}\varphi' \tag{41}$$

$$= N\frac{6EIR^2}{L^3}\sin^2\frac{\varphi}{2} \tag{42}$$

$$= N\frac{3EIR^2}{L^3}(1-\cos\varphi) \tag{43}$$

This enters into Eq. (9) (n.b: to ensure $\mathcal{H} = 0$, $U_{fil}(\varphi_0)$ has to be subtracted) and yield the period T:

$$T(\varphi_0) = 4\int_0^{\varphi_0} \sqrt{\frac{JL^2\left(1-2\xi^2(1-\cos\varphi)\right)+MR^4\sin^2\varphi}{2L\left(1-2\xi^2(1-\cos\varphi)\right)\left(MgL^2\left(\sqrt{1-2\xi^2(1-\cos\varphi)}-\sqrt{1-2\xi^2(1-\cos\varphi_0)}\right)+3NEI\xi^2(\cos\varphi-\cos\varphi_0)\right)}}\,\mathrm{d}\varphi \tag{44}$$

4 Solutions

There are neither for the integral (14) nor for the equation of motion (17) closed-form solutions. For the integral it is not possible to extract J in front of the integral, because in the nominator J occurs in the first summand only. Therefore, only numerical integration can be applied for the whole integral. As well, there are no closed-form solutions of the ordinary differential equation (ODE) (17) because of the square roots and the trigonometric functions.

1. The equation $T - T_{exp}$ is solved iteratively. First, for approximately 30 oscillations, the mean value for T_{exp} is determined from the experiment, e.g. using the zeros of the laser for the tangential movement. With this value T_{exp} an initial solution J_0 is calculated with the solution of the linear Eq. (20). As the period T increases with increasing amplitude φ_0 (cf. Uhler (1923)), for $T(\varphi_0)$ (calculated with J_0 and the value φ_0 from the experiment) holds $T(\varphi_0) < T_{exp}$. This means, that J_0 is a lower bound for the J, and increasing J_0 in steps, e.g. with $\Delta J = J_0/100$ until $T(\varphi_0) > T_{exp}$ gives a start interval for a bisection method.
2. Alternatively to the numerical integration of step 1, a series expansion of Uhler (1923), which is described in the appendix, can be used. This approach does not yield an analytical solution.
3. The third method is the simple application of a numerical algorithm for solving the ordinary differential Eq. (17).

Although we decided to use steel wire ropes, for the sake of completeness we compare different results with respect to the nonlinear behaviour with and without the bending stiffness of the φ_0-dependency of T. Furthermore, we compare methods 1., 2., and 3.

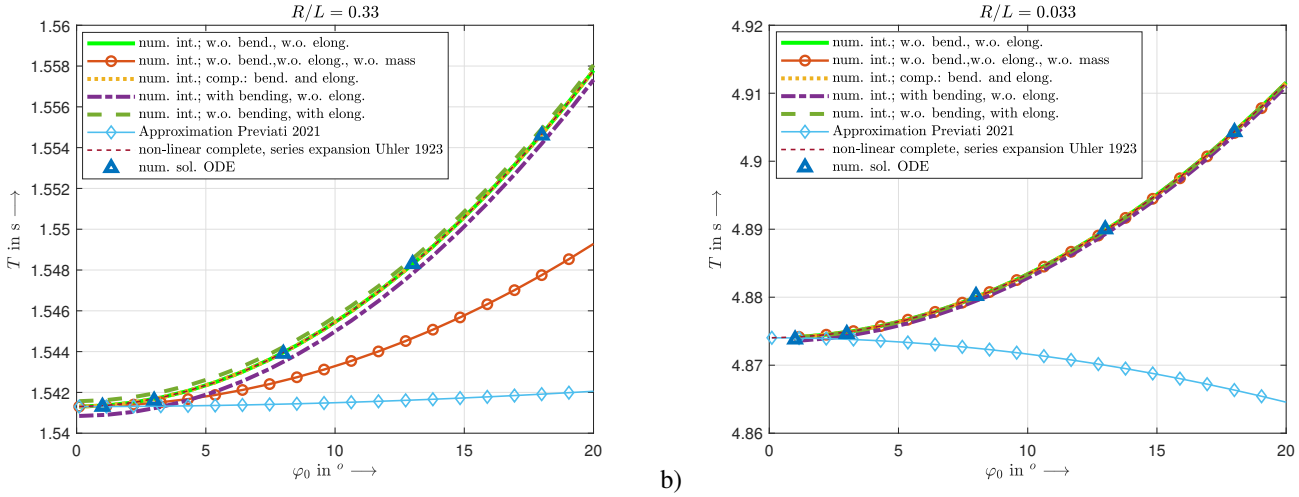

Fig. 5: Comparison of different calculations of the period T; a) $\xi = 0.33$, b) $\xi = 0.033$.

In Fig. 5 the function $T(\varphi_0)$ is shown for different approaches. All curves without literature citations (curve 1 to 4) show the results of the numerical integration of Eq. (44). The parameters are: $J = 1.8$ kg m^2, $M = 28$ kg, $R = 0.33$ m, $L = 1$ m for a), $L = 10$ m for b), $E = 210$ GPa, $r = r_{opt}$ from Eq. (39), $N = 3$, $g = 9.81$ m/s^2.

- Curve 1 (num. int.:w.o. bending, w.o. elong.): the numerical integration of Eq. (44) without the influence of bending and without the consideration of the elongation, i.e. $EI = 0$, $L = L_0$.
- Curve 2 (num. int.; w.o. bend., w.o. elong., w.o. mass): without the influence of bending, without the consideration of the elongation, without the influence of the translational kinetic energy of the mass M, i.e. $EI = 0$, $L = L_0$, and without the term $MR^4\sin^2\varphi$ in Eq. (44).

- Curve 3 (num. int.; comp.: bend. and elong.): the influence of the bending moments as well as the elongation is considered, the radius of the filars is calculated from Eq. (39), i.e. $EI \neq 0$, $L = L_0 + \Delta L$
- Curve 4: (num. int.; with bend., w.o. elong.): with the influence of bending and without the consideration of the elongation, i.e. $EI \neq 0$, $L = L_0$.
- Curve 5 (num. int.; w.o. bending, with elong.): without the influence of bending and with the consideration of the elongation, i.e. $EI = 0$, $L = L_0 + \Delta L$.
- Curve 6 Approximation from Previati (2021): Neither bending nor elongation is considered, i.e. $EI = 0$, $L = L_0$.
- Curve 7 Approximation from Uhler (1923): Neither bending nor elongation is considered, i.e. $EI = 0$, $L = L_0$.
- Data points 8: Numerical solutions of the ODE (without bending and without elongation). As the ODE (17) is not given in a simple, explicit form, we use an solver for implicit ODE. Important is, that a high precision and a maximum stepsize is prescribed for the algorithm.

a) For the short length $L = 1$ m of the filars, the solution of Eq. (44) a) and for five amplitudes the periods of the solution of (17) are shown in Fig. 5. It is obvious, that the numerical integration of Eq. (44), curve 1, compared to the the series expansion of Uhler (1923), curve 7, are identical within the coat line. The compensation of the bending stiffness by considering the elongation is visible in curve 3: this curve fits as well very good to curve 1, which shows, that the compensation is not only valid for the linearised but for the nonlinear equation, too. In order to demonstrate the influence of the bending stiffness and the elongation, these two effects are separated and visualized with the curve 4 (bending, no elongation) and 5 (no bending, elongation). It is feasible, that the bending stiffness results in smaller values for T, whereas the elongation results in larger one.

   It is notable, that skipping the translational kinetic energy in the vertical direction in the derivation of Eq. (44) results in significant deviations of the periods, cf. curve 2, especially for large amplitudes. The same holds for the approximation of Previati (2021). These deviations increase with an decreasing radius of gyration $\sqrt{J/M}$.

   The solutions from the numerical integration of the ODE (17) are very close to the numerical solution of Eq. (44) and the series expansion of Uhler (1923).

   The influence of the amplitude on the period between $\varphi_0 = 0^o$ and $\varphi_0 = 20^o$ is approximately 1.1 %.

b) For the large length $L = 10$ m all solutions despite the approximation of Previati (2021) have very small deviations to each other.

   For this long filars, the influence of bending and elongation is very small, there are nearly no differences between curve 4 and 5.

   Notable is the qualitative not appropriate behaviour of the approximation of Previati (2021): the period decreases with increasing amplitude.

   The influence of the amplitude on the period between $\varphi_0 = 0^o$ and $\varphi_0 = 20^o$ is approximately 0.7 %.

From this investigation we conclude:

1. If possible, one should prefer long filars in order to reduce the influence of bending, elongation and amplitude.
2. The calculation of the period using the numeric integration of the integral Eq. (44) is the preferable method. If there are no significant bending or torsion stiffness, which has to be considered, the series expansion of Uhler (1923) can be applied, too.
3. Solving the ODE (17) should be used very carefully, because, resulting from numerics, the calculated periods can fluctuate significantly. Therefore, the step size should be limited. Of course, in the case of relevant damped system, this is the only way to solve the system and to obtain a period, but the computer resources are significantly higher (depending on the precision) than method 2.
4. The approximation of Previati (2021) should not be used.

5 Experimental Results

In this section we will compare some results from the measurements to the numerical integration of Eq. (44) with $EI = 0$ and the measured length L. The parameters are:

a) $J = 1.7952$ kg m^2, $M = 27.759$ kg, $R = 0.33$ m, $L = 10.94$ m, $g = 9.81$ m/s^2 (cf. Fig. 6 a))
b) $J = 1.8024$ kg m^2, $M = 28.1040$ kg, $R = 0.33$ m, $L = 10.94$ m, $g = 9.81$ m/s^2 (cf. Fig. 6 b))

The parameters result from the measurement of the moment of inertia and the mass of the platform. The (artificial) object of investigation consists (s. Fig. 6) of two steel cylinders (mass each approx. 12 kg), two aluminium ITEM-profiles mounted on the cylinders and a Metawell-plate[3] between the profiles (height 150 mm in Fig. 6 a) and 300 mm in b)). The objects of investigation are geometrically measured and their weights were measured, too. Then the cylinders are symmetrically placed on the platform and the moment of inertia is calculated using the geometry and the masses. The overall moment of inertia and the total mass is a result of an addition.

[3]The plates of different heights damp the oscillations.

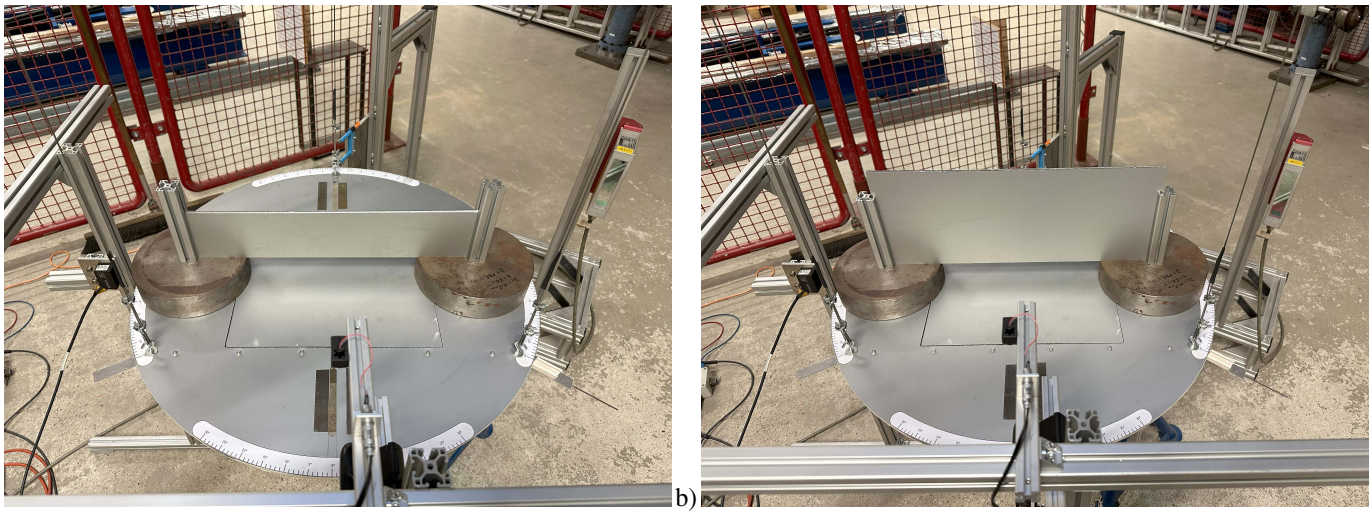

Fig. 6: Reference object of investigation: a) 150mm height of the damping plate; b) 300 m height of he damping plate

The experimental results for the two plates and the corresponding numerical solutions of the integral Eq. (44) are shown Fig. 7 and Fig. 8.

In both figures the solid blue graphs are the result of the numerical calculation of the integral Eq. (44) for the above mentioned parameters. The green triangles result from the solution of the ODE (17) without and the blue circles with damping (the latter symbols are skipped in Fig. 8).

The experimental data are marked by purple diamonds. Obviously, the experimental periods are approx. 0.9% to 1.2% higher than the calculated values. There might be several reasons for the deviations.

The most likely reason is a small deviation in the placement of the cylinders (Mass: $\approx$ 12 kg, distance from the rotation axis: $\approx$ 0.25 m): Assuming the nominal distance between a cylinder and the centre of the platform is exact 0.25 m and the deviation is 1 mm, this results in a deviation of the moment of inertia of $\Delta J \approx 0.012$ kg m^2 for the two cylinders. In Fig. 7 and Fig. 8, diagram a) the moment of inertia is increased in steps of $\Delta J = 0.012$ kg m^2. The change in the curves can nearly explain the deviations of the mean experimental results.

The measurement of the actual length of the filars is very difficult. It is likely, that in these measurements, too, errors may occur. Small increases of 10 mm or 20 mm of the length L results as well in a decrease of the deviations.

The damping, which is not considered in Eq. (44), is supposed to be a reason, too. To check this assumption, a linear damping term was introduced in the ODE (17). If we choose for the damping constant 0.05 Nms/rad (which is much higher than in the experiments) the periods decrease marginal (s. the blue circles in Fig. 7). Thus, the damping is very unlikely the reason. Furthermore, the damping for all the experiments are very low: the decay constants are $\delta = 0.00021$ 1/s (no plate), $\delta = 0.00033$ 1/s (plate of height of 150 mm), and $\delta = 0.00041$ 1/s (plate of height of 300 mm).

A fourth reason could be the nonlinear coupling between the rotation of the platform and the small translational movements in $\vec{e}_x$- and $\vec{e}_y$-direction. This possible reason has not yet been investigated. Some experimental modifications have been applied, to reduce the parasitic oscillations (e.g. mechanical and removable centring, or switchable eddy current damping). The initial amplitudes of the parasitic translational motions are approx. 0.2 -0.3 mm.

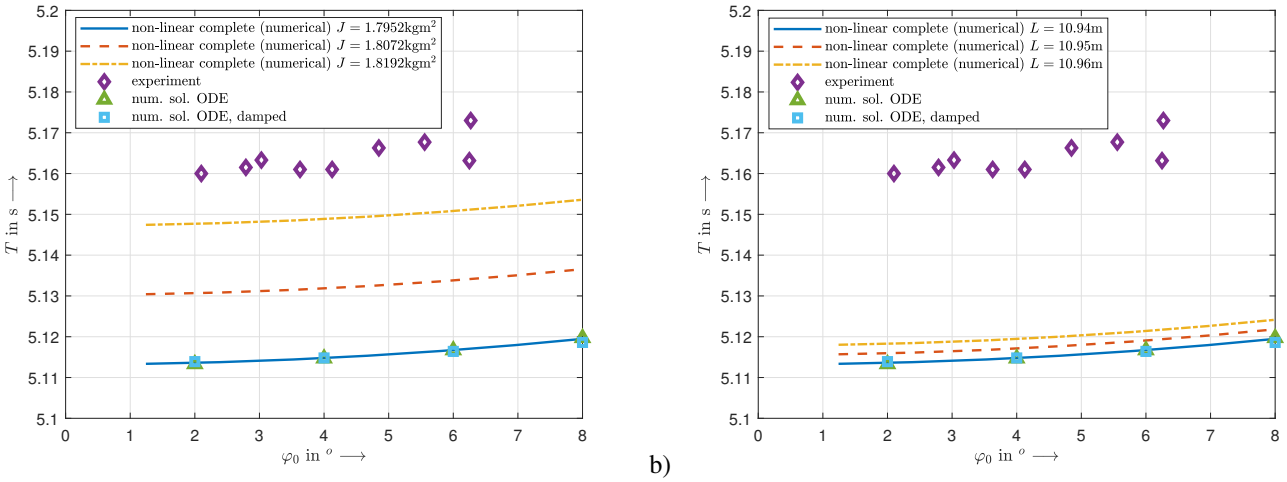

Fig. 7: Comparison of different calculations (numerical calculation of Eq. (44) and numerical integration of (17) of the period T; a) small variation of J, b) small variation of L for the dampingplate with 150 mm height (cf. Fig. 6 a))

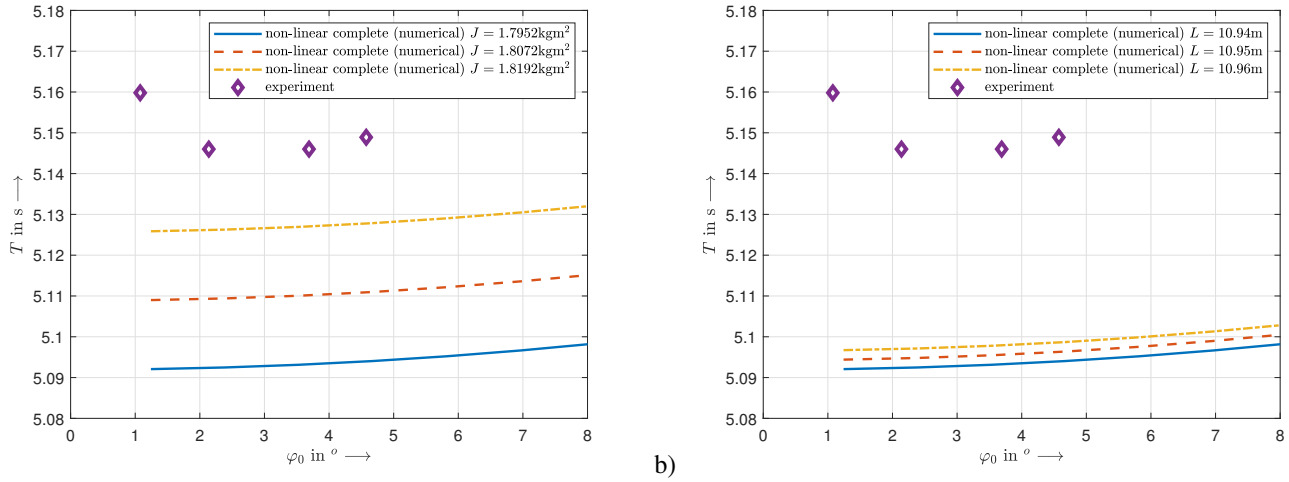

a) b)

Fig. 8: Comparison of different calculations (numerical calculation of Eq. (44) and numerical integration of (17) of the period T; a) small variation of J, b) small variation of L for the dampingplate with 300 mm height (cf. Fig. 6 b))

6 Conclusion

Different methods for the necessary evaluation of the period measurement of trifilar pendulums are described and compared to each other. It turns out, that all three solution methods are appropriate for a weakly damped system. The numerical integration and the series expansion are easier to apply and need less computer time than the numerical solution of the ordinary differential equation. If bending or torsion stiffness of the filars has to be considered, the series expansion from the literature has to be extended. For a large length of the filars the influence of bending and torsion stiffness is small. For large damping, only the numerical solution of the ordinary differential equation is applicable.

The deviations between the different methods except Previati (2021) are very small for small ratios R/L; for $R/L = 0.033$ the qualitative behaviour of the method of Previati (2021) is not correct. The experimental results for the periods are approx. 1 % higher than the calculated ones (which is known e.g. from Genta and Delprete (1994)), the reasons for these deviations are not clear and needs further investigations.

Appendix

A.1 Series Expansion of Uhler (1923)

Uhler (1923) gives a series expansion of the period T for a bifilar pendulum. As he uses a different variable ψ (cf. Fig. 2) for the description of the pendulum, his series expansion is not applicable to a pendulum with restoring torques from bending (and torsion). Nevertheless, his series expansion up to the third summand is very close to the numerical solution of the integral. With $\xi = R/L$ and $\kappa = \sqrt{J/M}/L$ the coefficients in the series expansion are:

$$a_0 = \frac{\kappa}{\xi} \tag{A.1}$$

$$b_1 = \frac{4\xi^4 - 3\xi^2\kappa^2 + \kappa^2}{2\xi^2\kappa^2} \tag{A.2}$$

$$b_2 = \frac{-16\xi^8 + 24\xi^6\kappa^2 - 5\xi^4\kappa^4 - 8\xi^4\kappa^2 - 10\xi^2\kappa^4 + 3\kappa^4}{8\xi^4\kappa^4} \tag{A.3}$$

$$b_3 = \frac{64\xi^{12} - 144\xi^{10}\kappa^2 + 92\xi^8\kappa^4 - 7\xi^6\kappa^6 + 48\xi^8\kappa^2 - 8\xi^6\kappa^4 + 7\xi^4\kappa^6 - 4\xi^4\kappa^4 - 21\xi^2\kappa^6 + 5\kappa^6}{16\xi^6\kappa^6} \tag{A.4}$$

The period is:

$$T = \frac{2\pi}{R}\sqrt{\frac{JL}{Mg}}\left(1 + \frac{1}{2}b_1 \sin^2\frac{\varphi_0}{2} + \frac{1\cdot 3}{2\cdot 4}b_2 \sin^4\frac{\varphi_0}{2} + \frac{1\cdot 3\cdot 5}{2\cdot 4\cdot 6}b_3 \sin^6\frac{\varphi_0}{2} + \ldots\right) \tag{A.5}$$

A.2 Approximation of Previati (2021)

Previati (2021) gives an approximation of the period T taking into account the torsion stiffness of the filars. Unfortunately, he applies some doubtful approximations of trigonometric functions, and the qualitative behaviour, i.e. increasing period T with an increasing amplitude φ_0, is not correct for all parameter combinations. The approximation is (k is the sum of all torsion stiffnesses

of the filars):

$$A = \frac{MR^4}{L^2} \tag{A.6}$$

$$B = \frac{MgR^2}{L} \tag{A.7}$$

$$C = \frac{1}{6} - \frac{R^2}{2L^2} \tag{A.8}$$

$$T = 2\pi \sqrt{\frac{J + \frac{1}{2}A\varphi_0^2}{k + B\left(1 + \frac{3}{4}C\varphi_0^2\right)}} \tag{A.9}$$

References

F. Auerbach. Pendel: E. bifilare aufhängung. In A. Winkelmann, editor, *Handbuch der Physik*, volume I, pages 413–414, 1908.

J. Awrejcewicz. *Classical Mechanics: Dynamics*. Springer, New York etc., 2012. doi: 10.1007/978-1-4614-3740-6.

R. M. Dreizler and C. S. Lüdde. *Theoretische Physik 1: Theoretische Mechanik*. Springer, Berlin, Heidelberg, 2008. doi: 10.1007/978-3-540-70558-1.

C. F. Gauß. Iv. anleitung zur bestimmung der schwingungsdauer einer magnetnadel. In C. F. Gauß and W. Weber, editors, *Beobachtungen des magnetischen Vereins im Jahre 1837*, pages 58–80, 1838.

G. Genta and C. Delprete. Some considerations on the experimental determination of moments of inertia. *Meccanica*, 29:125–141, 1994. doi: https://doi.org/10.1007/BF01007497.

M. Gobbi, G. Mastinu, and G. Previati. A method for measuring the inertia properties of rigid bodies. *Mechanical Systems and Signal Processing*, 25(1):305–318, 2011. ISSN 0888-3270. doi: https://doi.org/10.1016/j.ymssp.2010.09.004. URL https://www.sciencedirect.com/science/article/pii/S0888327010003092.

Z.-C. Hou, Y. n. Lu, Y. x. Lao, and D. Liu. A new trifilar pendulum approach to identify all inertia parameters of a rigid body or assembly. *Mechanism and Machine Theory*, 44(6):1270–1280, 2009. ISSN 0094-114X. doi: https://doi.org/10.1016/j.mechmachtheory.2008.07.004. URL https://www.sciencedirect.com/science/article/pii/S0094114X08001493.

P. E. Klopsteg. The bifilar pendulum. *Rev. Sci. Instr.*, 1(1):3–8, 1930.

R. Klöpper, M. Okuma, and J. Krüger. Neues verfahren zur messung vollständiger trägheitseigenschaften. *MTZ*, 74:249–245, 2013. doi: https://doi.org/10.1007/s35146-013-0056-z.

F. Kohlrausch. Absolute messung mittels bifilarer aufhängung, insbesondere zwei methoden zur bestimmung der erdrnagnetischen horizontalitensität ohne zeitmessmg. *Annalen der Physik und Chemie*, XVII(13):737–772, 1882.

D. P. Lyons. Obtaining optimal results with filar pendulums for moment of inertia measurements. In *61st Annual Conference, Virginia Beach, Virginia, May 18-22*, number 3237 in SAWE, page 29, Virginia Beach, Virginia, 2002. Society of Allied Weight Engineers, Inc.

G. Previati. Large oscillations of the trifilar pendulum: Analytical and experimental study. *Mechanism and Machine Theory*, 156: 104157, 2021. ISSN 0094-114X. doi: https://doi.org/10.1016/j.mechmachtheory.2020.104157. URL https://www.sciencedirect.com/science/article/pii/S0094114X20303748.

H. S. Uhler. Period of the bifilar pendulum for large amplitudes. *J. Opt. Soc. of Am. a. Rev of Sci. Instr.*, 7(3):263–274, 1923.

D. Wegener. Vehicle inertia measurement machine (vimm). In *Society of Allied Weight Engineers-71st International Conference on Mass Properties*, pages 153–162, 2012.